Published in final edited form as:
Proteins. 2011 November ; 79(11): 3123–3131. doi:10.1002/prot.23141.

Structural and Biochemical Analysis of Mammalian Methionine Sulfoxide Reductase B2

Finn L. Aachmann[a], **Geun-Hee Kwak**[b], **Rebecca Del Conte**[c], **Hwa-Young Kim**[b], **Vadim N. Gladyshev**[d], and **Alexander Dikiy**[a,*]

[a]Department of Biotechnology, Norwegian University of Science and Technology, Trondheim, N-7491, Norway

[b]Department of Biochemistry and Molecular Biology, Yeungnam University College of Medicine, Daegu, 705-717, Republic of Korea

[c]CERM, University of Florence, Sesto Fiorentino, 50019, Florence, Italy

[d]Genetics Division, Department of Medicine, Brigham and Women's Hospital and Harvard Medical School, Boston, MA 02115, USA

Abstract

Methionine sulfoxide reductases are antioxidant enzymes that repair oxidatively damaged methionine residues in proteins. Mammals have three members of the methionine-R-sulfoxide reductase family, including cytosolic MsrB1, mitochondrial MsrB2 and endoplasmic reticulum MsrB3. Here, we report the solution structure of reduced *Mus musculus* MsrB2 using high resolution NMR spectroscopy. MsrB2 is a β-strand rich globular protein consisting of eight all anti-parallel β-strands and three N-terminal α-helical segments. The latter secondary structure elements represent the main structural difference between mammalian MsrB2 and MsrB1. Structural comparison of mammalian and bacterial MsrB structures indicates that the general topology of this MsrB family is maintained and that MsrB2 more resembles bacterial MsrBs than MsrB1. Structural and biochemical analysis supports the catalytic mechanism of MsrB2 that, in contrast to MsrB1, does not involve a resolving cysteine (Cys). pH dependence of catalytically relevant residues in MsrB2 was accessed by NMR spectroscopy and the pK_a of the catalytic Cys162 was determined to be 8.3. In addition, the pH-dependence of MsrB2 activity showed a maximum at pH 9.0, suggesting that deprotonation of the catalytic Cys is a critical step for the reaction. Further mobility analysis showed a well-structured N-terminal region, which contrasted with the high flexibility of this region in MsrB1. Our study highlights important structural and functional aspects of mammalian MsrB2 and provides a unifying picture for structure-function relationships within the MsrB protein family.

Keywords

oxidoreductases; NMR spectroscopy; protein's structure and catalytic mechanism

Introduction

The sulfur-containing amino acid residue, methionine, is highly susceptible to oxidation by reactive oxygen species. Oxidation of methionine may damage proteins and impact on protein structure and function, but it can be reversed by the antioxidant repair enzymes,

*Corresponding author: Tel.:+4773597863, Fax: +4773591283; alex.dikiy@biotech.ntnu.no.

methionine sulfoxide reductases (Msrs) [1,2]. In addition, cyclic methionine oxidation/reduction is thought to be an important mechanism that protects cells against oxidative stress [3,4]. It is now well established that Msrs function as both important cellular antioxidants and protein repair enzymes. They have also been implicated in cellular signaling [5], regulation of lifespan [6–8], and protection against neurodegenerative diseases, such as Alzheimer's and Parkinson's diseases [9–11]. Recent studies showed that Msrs regulate mitochondrial functions in yeast [12] and modulate the TRAM6 channel during oxidative stress [13].

Methionine sulfoxide (Met-O) occurs as two epimers, Met-*S*-O and Met-*R*-O because of the chiral property of its sulfur atom. Two distinct Msr families evolved for the specific reduction of these two stereomers, including MsrA that is specific for Met-*S*O and MsrB that acts on Met-*R*-O. MsrA and MsrB have a catalytic cysteine (Cys) residue that attacks the sulfoxide moiety and share a catalytic mechanism involving a common sulfenic acid chemistry [14–19]. Msrs can be divided into two groups according to their catalytic mechanism: one has a resolving Cys residue (2-Cys Msrs) and the other lacks it (1-Cys Msrs). In 2-Cys Msr, the catalytic Cys sulfenic acid interacts with the resolving Cys to yield an intramolecular disulfide bond; the disulfide is then reduced by reductants such as thioredoxin (Trx) *in vivo* and dithiothreitol (DTT) *in vitro*, regenerating the enzyme for the next reaction cycle. In contrast, in 1-Cys Msrs, the catalytic Cys sulfenic acid is directly reduced by these reductants [15,16,20].

In mammalian cells, there are one MsrA and three MsrB proteins. MsrB1 is a cytosolic and nuclear selenoprotein and contains a resolving Cys in the N-terminal region. MsrB2 is a mitochondrial protein, and MsrB3 is located in the endoplasmic reticulum [21,22]. Both MsrB2 and MsrB3 belong to a 1-Cys Msr group (i.e., they lack a resolving Cys). We previously characterized biochemical and functional properties of mammalian MsrBs and examined their catalytic mechanisms [14–16,21]. Our recent structural analysis of MsrB1 provided insights into fold evolution and catalytic mechanism of selenoprotein MsrBs [23]. Here, we report an NMR structure of mouse MsrB2 and the biochemical analyses of this protein.

Materials and Methods

Sample preparation

Cloning, protein expression, and purification of uniformly isotope labeled (^{15}N or ^{15}N/^{13}C) recombinant mouse MsrB2 lacking the 44 N-terminal residues (45–175) and containing a C-terminal His-tag as well as conditions for NMR measurements were previously described [21,24]. NMR samples of the reduced protein contained 1–1.6 mM MsrB2 in 20 mM phosphate buffer (pH 6.0), 25 mM NaCl, and 5 mM DTT in 90% H_2O/10% D_2O or 99.9% D_2O.

NMR spectroscopy

NMR spectra were recorded at 298 K on a Bruker Avance 600 MHz spectrometer (at the Natural Sciences and Technology (NT) faculty NMR center of the Norwegian University of Sciences and Technology (NTNU)) equipped with a 5 mm z-gradient CP-TCI(H/C/N) or Bruker Avance 800 MHz spectrometer (at the NMR center of the University of Florence) equipped with a 5 mm z-gradient CP-TCI(H/C/N). Three-dimensional ^{13}C- and ^{15}N-edited ^{1}H,^{1}H-NOESY spectra were recorded in D_2O and H_2O, respectively. NMR data were processed using Bruker XWinNMR, version 3.5. NMR spectral analysis was performed using CARA version 1.4.1/1.5.3 [25]. ^{15}N-{^{1}H} heteronuclear NOEs were derived with Protein Dynamic Center software version 1.0.0 from Bruker BioSpin based on two independently measured and integrated ^{15}N-^{1}H heteronuclear correlated spectra recorded

using enhanced sensitivity sequence employing pulsed field gradient [26] with and without ^{1}H saturation. Nuclear magnetic relaxation (T_1 and T_2) measurements of ^{15}N nuclei were analyzed with Protein Dynamic Center software version 1.0.0 from Bruker BioSpin based on exponential fitting data in ^{15}N-HSQC spectra acquired with different relaxation delays [26,27].

Structure calculation

NOE cross peaks were identified, assigned and integrated in the aforementioned NOESY spectra using the program NEASY in CARA suite [25]. CALIBA [28] subroutine in CYANA 2.1 was used to convert cross peak intensities from NOESY spectra into distance constraints. Dihedral angle constraints were obtained from secondary chemical shifts with the TALOS program [29]. Zinc ion was incorporated into the MsrB2 structure as described for MsrB1 [23]. Based on the input described, the structure was calculated using the torsion angle dynamics program CYANA 2.1 [30]. Structure calculations started from 96 conformers with random torsion angle values. The 20 conformers with the lowest final CYANA target function values were energy-minimized in explicit water (shell of water molecules extending 12 Å in every direction from the protein surface resulting in the introduction of about 15000 water molecules) using the Amber force field with the aid of the AMBER 10 program [31]. The distance and torsion angle constraints were applied with force constants of 50 kcal·mol^{-1}·Å^{-2} and 32 kcal·mol^{-1}·rad^{-2}, respectively.

pH-dependence

pH titration of MsrB2 was performed on uniformly labeled $^{13}C/^{15}N$ ~1.0 mM MsrB2 in 20 mM phosphate buffer with 25 mM NaCl and 5 mM DTT in 90% H_2O/10% D_2O in the pH range 4.5–10.0 in steps on 0.5 pH units. Premade buffer solutions with certain pH values (pH value with 0.5 pH unit steps) were used to wash MsrB2 three times in a Vivaspin spin column and pH was checked prior to recording NMR spectra. This procedure ensured minimal change in ionic strength and well-defined pH values for each titration step. A ^{15}N-HSQC spectrum was recorded for each titration point.

Activity measurements

Reaction mixtures for activity assays (100 μl) contained 100 mM sodium phosphate (pH 5.7, 6.5, 7.0 or 7.5), 50 mM Tris-HCl (pH 7.6, 8.0, 8.6, or 9.0), or 50 mM carbonate-bicarbonate (pH 9.2, 9.6, or 10.0), 200 μM dabsyl-Met-*R*-O, 20 mM DTT, and 1 μg MsrB2. The reaction was carried out at 37°C for 30 min and the product, dabsyl-Met, was analyzed by the established HPLC procedure [32].

Determination of kinetic parameters

A C98S mutant was generated, in which Cys98 was replaced with Ser by site-directed mutagenesis. Purified wild type and C98S mutant MsrB2s were assayed in DTT- and Trx-dependent reactions. In the DTT-dependent reaction, the reaction mixture (100 μl) contained 50 mM sodium phosphate (pH 7.5), 50 mM NaCl, 20 mM DTT, 25–400 μM dabsyl-Met-*R*-O, and 1 μg purified protein. In the Trx-dependent reaction, the reaction mixture (100 μl) contained 50 mM sodium phosphate (pH 7.5), 50 mM NaCl, 0.2 mM NADPH, 6 μg yeast Trx1 [33], 3 μg human Trx reductase 1 [15], 25–400 μM dabsyl-Met-*R*-O, and 10 μg purified proteins. K_m and V_{max} values were determined by non-linear regression using GraphPad Prism 5 software.

Results and Discussion

Structure description

The solution structure of mouse MsrB2 was calculated based on the NOE-derived geometrical constraints, TALOS [29]-derived dihedral angles and distance constraints for the tetrahedral coordinated Zn^{2+} ion obtained from X-ray structures of other Zn^{2+} ion coordinated Cys residues in tetrahedral coordination geometry [34,35,36]. The geometrical constraints used in the calculations are summarized in Table 1. In total, 1296 NOE-based upper limit distances, 132 torsion angle restraints, and 8 upper limit distances and 8 lower limit distances for Zn^{2+} ion coordination were used to derive the MsrB2 structure. The resulting MsrB2 family is represented by the best 20 structures calculated with the CYANA 2.1 program, which subsequently were subjected to energy-minimization using AMBER 10 in explicit water. The geometrical constraint and coordinate files of the minimized MsrB2 family are deposited in the PDB under accession code 2L1U.

The family for the energy-refined structures of MsrB2 conformers is depicted in Figure 1A, and the average structure with secondary structure elements is shown in Figure 1B and C (without Zn^{2+} coordination) and Figure 1D (with Zn^{2+}). Structural statistics data characterizing quality of the calculated structure are summarized in Table 1. The resulting MsrB2 structure represents the conformation of low energy with the structural data well fitted to the experimentally derived geometrical constraints.

MsrB2, according to the NMR structure, is a β-strand rich globular protein consisting of eight all anti-parallel β-strands and three N-terminal α-helical segments. The first 30 amino acids at the N-terminal end of the recombinant protein form α-helices: α_1(47–53), α_2(54–62), and α_3(68–73) (amino acid numbering is based on the full sequence of mouse MsrB2 including the N-terminal mitochondrial signal peptide that was not part of the recombinant protein). A kink or small disruption between the first and second helices is introduced by Pro53. The main structure consists of two β-sheets. The smaller β-sheet forming the protein's backside is made up of three strands: β_1(78–83), β_2(91–94) and β_8(168–173). The larger sheet forming the front side consists of five strands: β_3(104–107), β_4(122–127), β_5(134–139), β_6(147–152), and β_7(160–164). The two β-sheets face each other in the structure, and form a core that resembles an intermediate between β barrel and β sandwich structures. The front side β-sheet forms the protein's hydrophobic core through residues Phe106, Phe161 and Ile163 linking to the backside β-sheet hydrophobic amino acids Tyr81 and Phe91 at the bottom of the structure. The top part of MsrB2 is held together through the tetrahedral structural zinc. A more disordered region, consisting of 14 residues (amino acids 107–121) between β_2 and β_3 strands, connects frontside and backside β-sheets of the protein. Three β-turns are established and located between the β_1 and β_2, the β_3 and β_4, and the β_4 and β_5 strands. There is a long-hairpin loop between β_5 and β_6. The three α-helices lie along the protein's surface linking to the frontal and backside β-sheets.

Zinc-binding site

Earlier studies on mammalian and bacterial MsrBs revealed that many of these proteins contain a single zinc atom, and this metal ion plays a structural role [21,32,37–39]. The common zinc isotope is NMR silent, but the $^{13}C_\beta$ chemical shifts of Cys appeared to be sensitive to zinc coordination [40]. From the NMR assignment of MsrB2, the average chemical shift value of 32.37±0.88 ppm for $^{13}C_\beta$ of four out of eight Cys residues was observed. This observation is in good agreement with the previous data that the $^{13}C_\beta$ chemical shift of a reduced Cys, which does not coordinate a Zn ion, is, on average, 28.92±2.11 ppm, whereas $^{13}C_\beta$ chemical shifts for the zinc coordinating Cys are 30.89±1.01 ppm [40]. This analysis, along with previous structural and biochemical analyses, show that Cys83, Cys86,

Cys139, and Cys142 in the two CxxC motifs coordinate a Zn ion, validating the presence of this metal ion within the MsrB2 molecule (Figure 1D).

Catalytic site

The catalytic site of the mouse MsrB2 is shown in Figure 2. The catalytic Cys is Cys162 that is part of the conserved R-F/Y-C-I-N-S-sequence present in most MsrBs [14,17]. This catalytic residue is located at the lower end of the larger front side β-sheet (the middle of strand β_7). This β-sheet builds up a solvent exposed surface and thus the catalytic Cys162 is readily exposed to the solvent. The conserved Trp103 has been proposed as an important residue involved in stabilization and orienting the substrate by interacting with the ε-methyl group of the substrate [17,41]. A Cys-Arg-Asp/Glu triad has been implicated as an essential unity for activating the catalytic Cys in several MsrBs [17,42]. One aspartate (Asp152) and one arginine (Arg160) are indeed found near the catalytic Cys in the MsrB2 structure. These residues are the only charged amino acids in or near the catalytic thiol possibly involved either in substrate binding or stabilization of the active site topology. Furthermore, Phe150 is also close to Cys162, which, together with Trp103, can form a hydrophobic patch for possible stabilization of the bound substrate.

The reaction mechanism of MsrBs suggested earlier [14–16] implies that oxidized MsrB2 lacking a conserved resolving Cys is directly reduced by an appropriate electron donor (e.g., Trx *in vivo* or DTT *in vitro*). It was previously reported [43] that in a bacterial MsrB from *Xanthomonas campestris* lacking the conserved resolving Cys, an N-terminal Cys31 residue could form a disulfide bridge with the catalytic Cys and thus act as a resolving Cys due to high flexibility of the N-terminal region. Based on the calculated MsrB2 structures the only possible candidate for a resolving Cys is Cys98, which is localized in the loop next to the active site. In the structure, the side chain of Cys98 is oriented away from Cys162 and the distance between Sγ-Sγ (Cys98-Cys162) ranges from 8.6 to 17.6 Å. Due to a possible flexibility of the loop containing Cys98, the hypothesis whether Cys98 can function as a resolving Cys in MsrB2 was tested. A C98S mutant, in which Cys was replaced with Ser, was generated and its kinetic parameters were determined (Table 2). In the DTT-dependent assay, V_{max} and K_m values of the C98S mutant were slightly higher than those of the wild type protein. In the Trx-dependent assay, the C98S mutant had 6-fold and 10-fold higher V_{max} and K_m values, respectively, relative to the wild-type protein. We conclude that Cys98, does not act as a resolving Cys in the MsrB2 reaction. These biochemical data support the catalytic mechanism of 1-Cys MsrB2 wherein the catalytic Cys sulfenic acid is directly reduced by reductants (e.g., thioredoxin) to regenerate the enzyme for the next catalytic cycle.

Electrostatic surface potential

The electrostatic surface potential for MsrB2 was calculated at neutral pH and the results are shown in Figure 1E. It appears that the front side of MsrB2, around the active site, is mainly neutral and the charges are equally distributed over the rest of the frontal surface. This correlates well with the observation that mainly hydrophobic amino acids surround the active site. Hydrophobic interactions evidently play an important role in stabilization of the substrate-protein complex during the catalytic reaction. In contrast, the protein backside is more charged (Figure 1E). Both positive and negative charges are distributed throughout the whole backside surface, with a small negative patch being located at the top of this region.

pH-dependence of residues relevant to catalysis

It was previously shown [44] that pK_a values of catalytic Cys117 and His103 residues (corresponding to Cys95/His80 and Cys162/His148, respectively, in mammalian MsrB1 and MsrB2 proteins) in the resting state of MsrB from *Neisseria meningitidis* are 9.3 and 6.6,

respectively, being only slightly shifted from the values of free amino acids [45]. The corresponding pK_a values for Cys95 and His80 in mammalian MsrB1 were found to be 6.0 and 5.7, respectively [23]. While pK_a values for the catalytically relevant His are closer to each other in the indicated bacterial and mammalian MsrBs and are also similar to the unperturbed pK_a value of His, the reported Cys95 pK_a value differed by more than two units when mammalian MsrB1 was compared with the *N. meningitidis* enzyme. The pH-dependence of MsrB1 activity determined from kinetic measurements correlates well with the pK_a value of 6.0 determined by NMR for Cys95 [23].

In contrast to MsrB1, mammalian MsrB2 is a Cys-containing protein. The calculated structure and its overall topology make this protein more similar to bacterial MsrBs rather than to mammalian MsrB1. To examine additional differences among mammalian MsrBs as well as between mammalian and bacterial proteins, we carried out measurements of pK_a values of catalytically relevant residues of MsrB2 using both NMR spectroscopy and kinetic assays. NMR spectroscopy was employed to monitor pH dependence of signals corresponding to the residues constituting the catalytic site. ^{15}N heteronuclear HSQC spectra of the protein were recorded at different pH values in the interval between 4.5 and 10.0. The data were analyzed by plotting the chemical shift values as a function of pH (Figure 3).

The pH titration profile for Cys162 (Figure 3A,B) has two acid-base transitions with pK_a of 8.3 and ~10. Based on structural inspection of MsrB2, the side chain of Arg160 situated in the vicinity of Cys162 (the distance is 6.1–11.3 Å between Cys162 Sγ-Arg160 C_ζ) could affect the titration profile of Cys162. The titration profile of Arg160 was examined and its pK_a seems to be close to 10 (data not shown), which fits well with the titration profile for Cys162. The pK_a value of Cys162 transition was 8.3±0.3, from fitting the experimental data to the Henderson-Hasselbach equation. Comparison of this value to the corresponding value of MsrB1 revealed the difference of 2.3 units while 1.0 pH unit difference was observed between MsrB2 and *N. meningitidis* MsrB. To check whether the determined Cys162 pK_a correlates with the functional pK_a value, as it was found in the case of MsrB1 [23], the kinetic measurements were undertaken in the range of pH 5.7–10.0. The enzyme had a maximal catalytic activity at pH 9.0 (Table 3). This correlated well with the pK_a value of 8.3 determined for Cys162, suggesting that the catalytic activity of MsrB2 is regulated by deprotonation of Cys162.

Titration profile of His148 appears as a mixture of two transitions (Figure 3C,D) and the second transition may be due to deprotonation of the nearby catalytic Cys162 (the distance is 3.1–9.0 Å between Cys162 Sγ and His 148 C_ε). The pK_a value of His148 was calculated at 7.2±0.3 accounting for the effect of Cys162 deprotonation. This pK_a value is closer to the unperturbed pK_a value of His and is only 0.6 units away from the reported value for the *N. meningitidis* MsrB [44]. The difference between the corresponding pK_a values for catalytic His in mammalian MsrB1 [23] and MsrB2 proteins was 1.5 units.

Altogether, the pH-dependence measurements for mammalian MsrB1 [23] and MsrB2 are consistent with the idea that deprotonation of the catalytic selenocysteine (Sec) in MsrB1 or Cys in MsrB2 is an important step for regulating the activity of these proteins. This observation agrees with the proposed mechanism for Met-O reduction [14].

Mobility studies

The structure of MsrB1 revealed that it has a flexible N-terminal region containing a novel resolving Cys [23], while the MsrB2 structure has three α-helices in the N-terminal region. In order to obtain further information regarding intra-molecular dynamics of MsrB2, $^{15}N\{H\}$-NOE as well as T_1 and T_2 relaxation times were measured. These data suggested that the most N-terminal α-helices (47–53) and (54–62) are somewhat mobile while the third α-helix

(68–73) has the same average mobility as the protein core (Supplementary Figure S1). However, the observed decrease in the structural resolution for the N-terminal region of MsrB2 with respect to the rest of the protein is likely due to the intrinsically low number of NOE constraints between α-helices and the folded core of the protein. Overall, in contrast to MsrB1, MsrB2 essentially lacks mobility in the N-terminal region. Considering the mobility properties of MsrB1, in which the increased flexibility of the N-terminal region assists in the formation of an intramolecular disulfide between the N-terminal resolving Cys4 and the catalytic Sec95[23], and the present data, revealing that MsrB2 lacks the resolving Cys and restricts mobility of its N-terminal region, it is plausible to suggest that the mobility difference in the N-terminal regions between Sec-containing MsrB1 and Cys-containing MsrB2 can lead to different catalytic mechanisms adopted by these two proteins. The mobility studies also indicated that the loops between strands β_2 and β_3 and between strands β_4 and β_5 have slightly increased mobility compared to the rest of the protein. These two loops are located on each side of the active site and this increased flexibility may be needed to adjust the active site to different protein substrates.

Structural comparison

Previously, we carried out an initial comparative structural analysis of the MsrB protein family (without mammalian MsrB2) [23]. In the current study, we highlight the main points of the structural comparison involving MsrB2. The structures of mammalian and representative bacterial MsrBs that illustrate their secondary structure elements are shown in Figure 4. The overall structure topology of mammalian MsrB2, the subject of this report, is very similar to those of mammalian MsrB1 and bacterial MsrBs. Indeed, all these proteins show an ellipsoidal shape consisting of two anti-parallel β-sheets, and their catalytic Cys (or Sec) is surrounded with two/three charged residues (Arg, Asp/Glu) involved in the activation of the catalytic residue. However, the comparison also shows that MsrB2 is more similar to bacterial MsrBs than to MsrB1 as it contains three α-helices on the exterior of the protein in the N-terminal region. These helices could be relevant for the interaction of MsrB2 with its protein substrates.

Concluding remarks

Herewith, a three-dimensional structure of mammalian mitochondrial MsrB2 obtained using high resolution NMR spectroscopy is reported. The overall structure is composed of two β-sheets consisting of eight anti-parallel β-strands and three N-terminal α-helices and is more similar to those of bacterial MsrBs than to that of mammalian MsrB1. The structural and biochemical analysis supports the catalytic mechanism involving no resolving Cys in the regeneration of MsrB2. In contrast to high flexibility of the N-terminal region of MsrB1, this region in MsrB2 is virtually immobile. This difference in mobility may lead to different catalytic mechanisms employed by the two mammalian MsrBs. The catalytic Cys162 pK_a is 8.3 as determined by NMR spectroscopy. This value is in a good agreement with the pH-dependence of enzyme activity. Comparison of structural and biochemical data for MsrB2 and MsrB1 [23] suggests that the activity of these proteins is modulated by protonation state of their catalytic Sec/Cys. In summary, the data provide a unifying picture of structural and functional properties within the mammalian MsrB family.

Supplementary Material

Refer to Web version on PubMed Central for supplementary material.

Acknowledgments

AD acknowledges the support from the NT Faculty, NTNU. Financial support in the form of access to the Bio-NMR Research Infrastructure co-funded under the 7th Framework Programme of the EC (FP7/2007–2013) grant agreement 261863 and project contract RII3-026145 for conducting the research is gratefully acknowledged. FLA acknowledges financial support from the Norwegian Research Council (NFR) via KMB project (182695/I40). This work was also supported by the National Research Foundation of Korea grant 2010-0001240 (to HYK) and NIH AG021518 (to VNG).

Abbreviations

NMR	Nuclear Magnetic Resonance
MsrB	Methionine sulfoxide reductase B
NOE	Nuclear Overhauser Effect
NOESY	Nuclear Overhauser Effect Spectroscopy
PDB	Protein Data Bank

References

1. Kim HY, Gladyshev VN. Methionine sulfoxide reductases: selenoprotein forms and roles in antioxidant protein repair in mammals. Biochem J. 2007; 407(3):321–329. [PubMed: 17922679]
2. Lee BC, Dikiy A, Kim HY, Gladyshev VN. Functions and evolution of selenoprotein methionine sulfoxide reductases. Biochim Biophys Acta. 2009; 1790(11):1471–1477. [PubMed: 19406207]
3. Levine MS, Li Z, Cepeda C, Cromwell HC, Altemus KL. Neuromodulatory actions of dopamine on synaptically-evoked neostriatal responses in slices. Synapse. 1996; 24(1):65–78. [PubMed: 9046078]
4. Luo S, Levine RL. Methionine in proteins defends against oxidative stress. FASEB J. 2009; 23(2): 464–472. [PubMed: 18845767]
5. Erickson JR, Joiner ML, Guan X, Kutschke W, Yang J, Oddis CV, Bartlett RK, Lowe JS, O'Donnell SE, Aykin-Burns N, Zimmerman MC, Zimmerman K, Ham AJ, Weiss RM, Spitz DR, Shea MA, Colbran RJ, Mohler PJ, Anderson ME. A dynamic pathway for calcium-independent activation of CaMKII by methionine oxidation. Cell. 2008; 133(3):462–474. [PubMed: 18455987]
6. Koc A, Gasch AP, Rutherford JC, Kim HY, Gladyshev VN. Methionine sulfoxide reductase regulation of yeast lifespan reveals reactive oxygen species-dependent and -independent components of aging. Proc Natl Acad Sci U S A. 2004; 101(21):7999–8004. [PubMed: 15141092]
7. Ruan H, Tang XD, Chen ML, Joiner ML, Sun G, Brot N, Weissbach H, Heinemann SH, Iverson L, Wu CF, Hoshi T. High-quality life extension by the enzyme peptide methionine sulfoxide reductase. Proc Natl Acad Sci U S A. 2002; 99(5):2748–2753. [PubMed: 11867705]
8. Minniti AN, Cataldo R, Trigo C, Vasquez L, Mujica P, Leighton F, Inestrosa NC, Aldunate R. Methionine sulfoxide reductase A expression is regulated by the DAF-16/FOXO pathway in Caenorhabditis elegans. Aging Cell. 2009; 8(6):690–705. [PubMed: 19747232]
9. Gabbita SP, Aksenov MY, Lovell MA, Markesbery WR. Decrease in peptide methionine sulfoxide reductase in Alzheimer's disease brain. J Neurochem. 1999; 73(4):1660–1666. [PubMed: 10501213]
10. Liu F, Hindupur J, Nguyen JL, Ruf KJ, Zhu J, Schieler JL, Bonham CC, Wood KV, Davisson VJ, Rochet JC. Methionine sulfoxide reductase A protects dopaminergic cells from Parkinson's disease-related insults. Free Radic Biol Med. 2008; 45(3):242–255. [PubMed: 18456002]
11. Oien DB, Osterhaus GL, Latif SA, Pinkston JW, Fulks J, Johnson M, Fowler SC, Moskovitz J. MsrA knockout mouse exhibits abnormal behavior and brain dopamine levels. Free Radic Biol Med. 2008; 45(2):193–200. [PubMed: 18466776]
12. Kaya A, Uzunhasan I, Baskurt M, Ozkan A, Ataoglu E, Okcun B, Yigit Z. Oxidative status and lipid profile in metabolic syndrome: gender differences. Metab Syndr Relat Disord. 2010; 8(1):53–58. [PubMed: 19958158]

13. Cao G, Lee KP, van der Wijst J, de Graaf M, van der Kemp A, Bindels RJ, Hoenderop JG. Methionine sulfoxide reductase B1 (MsrB1) recovers TRPM6 channel activity during oxidative stress. J Biol Chem. 2010; 285(34):26081–26087. [PubMed: 20584906]
14. Kim HY, Gladyshev VN. Different catalytic mechanisms in mammalian selenocysteine- and cysteine-containing methionine-R-sulfoxide reductases. PLoS Biol. 2005; 3(12):e375. [PubMed: 16262444]
15. Kim HY, Kim JR. Thioredoxin as a reducing agent for mammalian methionine sulfoxide reductases B lacking resolving cysteine. Biochem Biophys Res Commun. 2008; 371(3):490–494. [PubMed: 18452709]
16. Lee TH, Kim HY. An anaerobic bacterial MsrB model reveals catalytic mechanisms, advantages, and disadvantages provided by selenocysteine and cysteine in reduction of methionine-R-sulfoxide. Arch Biochem Biophys. 2008; 478(2):175–180. [PubMed: 18722338]
17. Lowther WT, Weissbach H, Etienne F, Brot N, Matthews BW. The mirrored methionine sulfoxide reductases of Neisseria gonorrhoeae pilB. Nat Struct Biol. 2002; 9(5):348–352. [PubMed: 11938352]
18. Boschi-Muller S, Azza S, Sanglier-Cianferani S, Talfournier F, Van Dorsselear A, Branlant G. A sulfenic acid enzyme intermediate is involved in the catalytic mechanism of peptide methionine sulfoxide reductase from Escherichia coli. J Biol Chem. 2000; 275(46):35908–35913. [PubMed: 10964927]
19. Boschi-Muller S, Gand A, Branlant G. The methionine sulfoxide reductases: Catalysis and substrate specificities. Arch Biochem Biophys. 2008; 474(2):266–273. [PubMed: 18302927]
20. Tarrago L, Laugier E, Zaffagnini M, Marchand CH, Le Marechal P, Lemaire SD, Rey P. Plant thioredoxin CDSP32 regenerates 1-cys methionine sulfoxide reductase B activity through the direct reduction of sulfenic acid. J Biol Chem. 2010; 285(20):14964–14972. [PubMed: 20236937]
21. Kim HY, Gladyshev VN. Methionine sulfoxide reduction in mammals: characterization of methionine-R-sulfoxide reductases. Mol Biol Cell. 2004; 15(3):1055–1064. [PubMed: 14699060]
22. Kim HY, Gladyshev VN. Characterization of mouse endoplasmic reticulum methionine-R-sulfoxide reductase. Biochem Biophys Res Commun. 2004; 320(4):1277–1283. [PubMed: 15249228]
23. Aachmann FL, Sal LS, Kim HY, Marino SM, Gladyshev VN, Dikiy A. Insights into function, catalytic mechanism, and fold evolution of selenoprotein methionine sulfoxide reductase B1 through structural analysis. J Biol Chem. 2010; 285(43):33315–33323. [PubMed: 20605785]
24. Breivik AS, Aachmann FL, Sal LS, Kim HY, Del Conte R, Gladyshev VN, Dikiy A. 1H, 15N and 13C NMR assignments of mouse methionine sulfoxide reductase B2. Biomol NMR Assign. 2008; 2(2):199–201. [PubMed: 19636904]
25. Keller, RLJ. Optimizing the Process of Nuclear Magnetic Resonance Spectrum Analysis and Computer Aided Resonance Assignment. Zürich: CANTINA Verlag; 2004.
26. Farrow NA, Muhandiram R, Singer AU, Pascal SM, Kay CM, Gish G, Shoelson SE, Pawson T, Forman-Kay JD, Kay LE. Backbone dynamics of a free and phosphopeptide-complexed Src homology 2 domain studied by 15N NMR relaxation. Biochemistry. 1994; 33(19):5984–6003. [PubMed: 7514039]
27. Kay LE, Torchia DA, Bax A. Backbone dynamics of proteins as studied by 15N inverse detected heteronuclear NMR spectroscopy: application to staphylococcal nuclease. Biochemistry. 1989; 28(23):8972–8979. [PubMed: 2690953]
28. Güntert P, Braun W, Wüthrich K. Efficient computation of three-dimensional protein structures in solution from nuclear magnetic resonance data using the program DIANA and the supporting programs CALIBA, HABAS and GLOMSA. J Mol Biol. 1991; 217(3):517–530. [PubMed: 1847217]
29. Cornilescu G, Delaglio F, Bax A. Protein backbone angle restraints from searching a database for chemical shift and sequence homology. J Biomol NMR. 1999; 13(3):289–302. [PubMed: 10212987]
30. Güntert P, Wüthrich K. Improved efficiency of protein structure calculations from NMR data using the program DIANA with redundant dihedral angle constraints. J Biomol NMR. 1991; 1(4):447–456. [PubMed: 1841711]

31. Case DA, Cheatham TE 3rd, Darden T, Gohlke H, Luo R, Merz KM Jr, Onufriev A, Simmerling C, Wang B, Woods RJ. The Amber biomolecular simulation programs. J Comput Chem. 2005; 26(16):1668–1688. [PubMed: 16200636]
32. Kumar RA, Koc A, Cerny RL, Gladyshev VN. Reaction mechanism, evolutionary analysis, and role of zinc in Drosophila methionine-R-sulfoxide reductase. J Biol Chem. 2002; 277(40):37527–37535. [PubMed: 12145281]
33. Kwak GH, Kim MJ, Kim HY. Cysteine-125 is the catalytic residue of Saccharomyces cerevisiae free methionine-R-sulfoxide reductase. Biochem Biophys Res Commun. 2010; 395(3):412–415. [PubMed: 20382110]
34. Colonna-Cesari F, Perahia D, Karplus M, Eklund H, Braden CI, Tapia O. Interdomain motion in liver alcohol dehydrogenase. Structural and energetic analysis of the hinge bending mode. J Biol Chem. 1986; 261(32):15273–15280. [PubMed: 3771574]
35. Mechulam Y, Schmitt E, Maveyraud L, Zelwer C, Nureki O, Yokoyama S, Konno M, Blanquet S. Crystal structure of Escherichia coli methionyl-tRNA synthetase highlights species-specific features. J Mol Biol. 1999; 294(5):1287–1297. [PubMed: 10600385]
36. Chantalat L, Leroy D, Filhol O, Nueda A, Benitez MJ, Chambaz EM, Cochet C, Dideberg O. Crystal structure of the human protein kinase CK2 regulatory subunit reveals its zinc finger-mediated dimerization. EMBO J. 1999; 18(11):2930–2940. [PubMed: 10357806]
37. Kryukov GV, Kumar RA, Koc A, Sun Z, Gladyshev VN. Selenoprotein R is a zinc-containing stereo-specific methionine sulfoxide reductase. Proc Natl Acad Sci U S A. 2002; 99(7):4245–4250. [PubMed: 11929995]
38. Boschi-Muller S, Olry A, Antoine M, Branlant G. The enzymology and biochemistry of methionine sulfoxide reductases. Biochim Biophys Acta. 2005; 1703(2):231–238. [PubMed: 15680231]
39. Gruez A, Libiad M, Boschi-Muller S, Branlant G. Structural and biochemical characterization of free methionine-R-sulfoxide reductase from Neisseria meningitidis. J Biol Chem. 2010; 285(32): 25033–25043. [PubMed: 20489204]
40. Kornhaber GJ, Snyder D, Moseley HN, Montelione GT. Identification of zinc-ligated cysteine residues based on 13Calpha and 13Cbeta chemical shift data. J Biomol NMR. 2006; 34(4):259–269. [PubMed: 16645816]
41. Kauffmann B, Aubry A, Favier F. The three-dimensional structures of peptide methionine sulfoxide reductases: current knowledge and open questions. Biochim Biophys Acta. 2005; 1703(2):249–260. [PubMed: 15680233]
42. Kim HY, Gladyshev VN. Role of structural and functional elements of mouse methionine-S-sulfoxide reductase in its subcellular distribution. Biochemistry. 2005; 44(22):8059–8067. [PubMed: 15924425]
43. Ranaivoson FM, Neiers F, Kauffmann B, Boschi-Muller S, Branlant G, Favier F. Methionine sulfoxide reductase B displays a high level of flexibility. J Mol Biol. 2009; 394(1):83–93. [PubMed: 19733575]
44. Neiers F, Sonkaria S, Olry A, Boschi-Muller S, Branlant G. Characterization of the amino acids from Neisseria meningitidis methionine sulfoxide reductase B involved in the chemical catalysis and substrate specificity of the reductase step. J Biol Chem. 2007; 282(44):32397–32405. [PubMed: 17766244]
45. Creighton, TE. Proteins - Structure and Molecular Properties. New York: W.H. Freeman and Company; 1996.
46. Li H, Robertson AD, Jensen JH. Very fast empirical prediction and rationalization of protein pK(a) values. Proteins. 2005; 61(4):704–721. [PubMed: 16231289]
47. Baker NA, Sept D, Joseph S, Holst MJ, McCammon JA. Electrostatics of nanosystems: Application to microtubules and the ribosome. Proc Natl Acad Sci USA. 2001; 98(18):10037–10041. [PubMed: 11517324]
48. DeLano, WL. The PyMOL Molecular Graphics System. Palo Alto, CA, USA: DeLano Scientific LLC; 2008.

49. Kim YK, Shin YJ, Lee WH, Kim HY, Hwang KY. Structural and kinetic analysis of an MsrA-MsrB fusion protein from Streptococcus pneumoniae. Mol Microbiol. 2009; 72(3):699–709. [PubMed: 19400786]

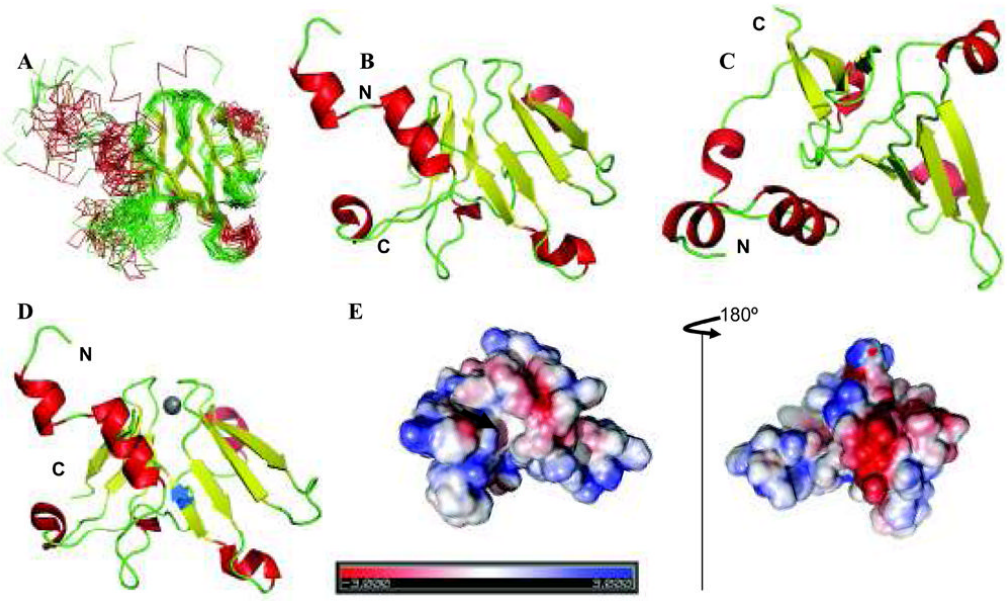

Fig. 1. Three-dimensional NMR structure of reduced mouse MsrB2

(A) The MsrB2 structural family consists of 20 conformers with the lowest target function. (B) and (C) Front and top orientations of MsrB2 with the lowest target function. (D) Frontal view of MsrB2 structure with the zinc ion indicated as grey sphere and the catalytic Cys162 highlighted as orange sticks. (E) Electrostatic surface potential of MsrB2: frontal and backside views, where the position of the catalytic Cys is indicated by a black arrow. The program PDB2PQR, version 1.5 [46], was used to prepare the structures for calculation of electrostatic potential distribution, which was performed with the program APBS at pH 7.0 with ionic strength of 0.4 M [47]. Visualization of the potential plotted on the solvent accessible surface was made with PyMol, version 0.99 [48]. Red and blue denote regions of negative (i.e., less than −3 kT/|e|) and positive (i.e., more than +3 kT/|e|) potentials on the MsrB2 surface, respectively. Structural models were prepared with PyMol, version 0.99[48].

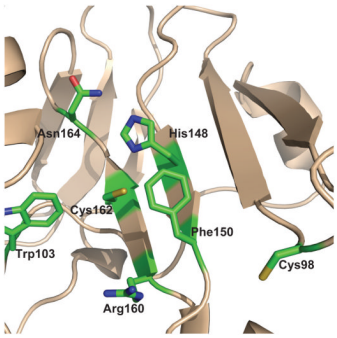

Fig. 2. Structure of the active site of mouse MsrB2 protein showing catalytically relevant residues

Cys98 is also shown. Our studies suggested that it does not serve as a resolving Cys in MsrB2.

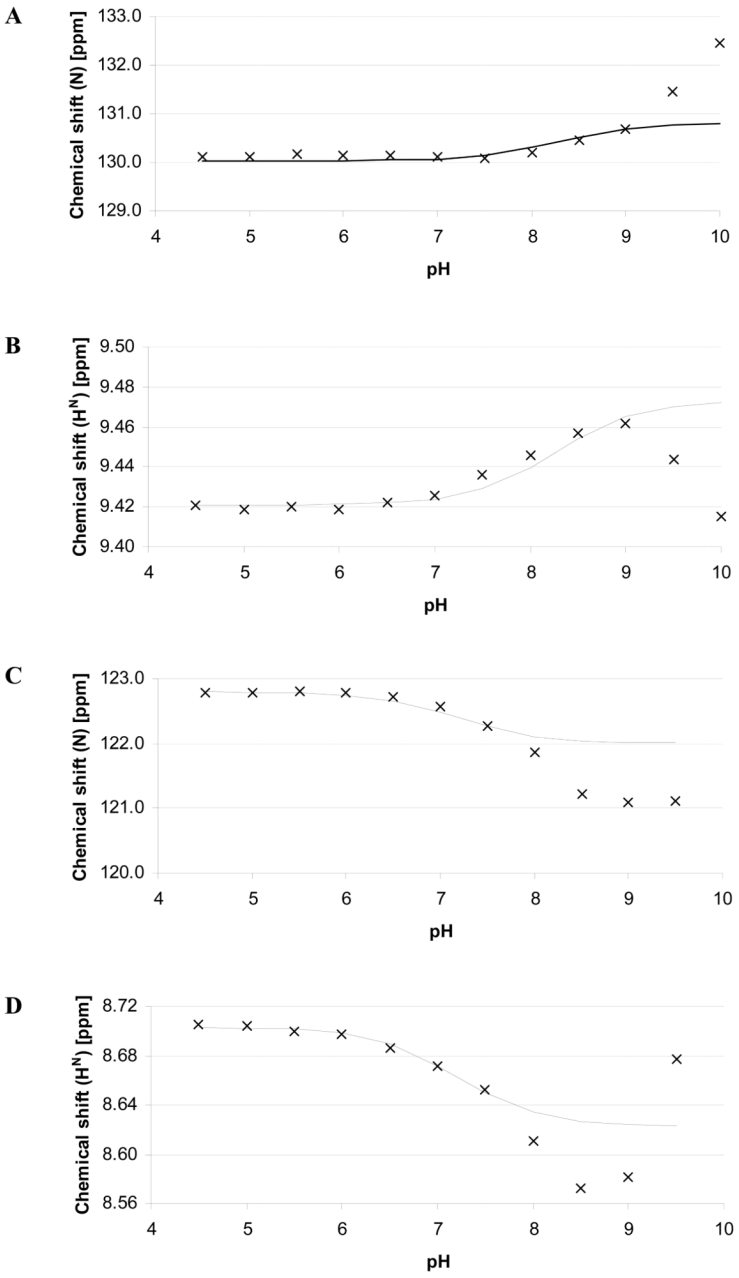

Fig. 3. Transition curves for titration of Cys162 and His148 in mouse MsrB2

(A) The proton chemical shift of H^N and (B) the backbone nitrogen chemical shift of Cys162 are plotted as a function of pH. (C) The proton chemical shift of H^N and (D) the backbone nitrogen chemical shift of His148 are plotted as a function of pH.

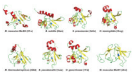

Fig. 4. Comparison of three-dimensional structures of MsrBs

Secondary structure elements are shown for each protein and the catalytic Cys residue is highlighted in blue. The figure includes *M. musculus* MsrB2 (2l1u) and MsrB1(2kvi)[23], and *Bacillus subtilis* (2kzn), *Stretococcus pneumoniae* (3e0o)[49], *Neisseria meningitidis* (3hcg)[43], *Methanothermobacter thermautotrophicus* (2k8d), *Burkholderia pseudomallei* (3cez), *Neisseria gonorrhoeae* (1l1d) MsrBs[23].

Table 1

Structural statistics and geometrical constraints derived from NMR for the reduced form of mouse MsrB2

	Number
Restraints used in structure calculation	
Total number of NOE distance restraints	1296
Intraresidual	606
Short range	474
Medium range	107
Long range	109
Number of lower limits for zinc ion	8
Number of upper limits for zinc ion	8
Torsion angle constraints	132
Structure statistics, 20 conformers	
CYANA target function value ($Å^2$)	4.00±0.48
Maximal distance constraint violation	0.49±0.11
Maximal torsion angle constraint violation	8.45±1.86
AMBER energies in water (kcal/mol)	−1.81E+5
PROCKECK-NMR Ramachandran statistics	
Residues in favorable regions (%)	73.4
Residues in additional allowed regions (%)	22.6
Residues in generously allowed regions (%)	2.9
Residues in disallowed regions (%)	1.2
RMSD to average coordinates (Å)	
N, C^{α}, C′ (4–130)	2.56±0.70
N, C^{α}, C′ (secondary structure)	3.14±0.75
Heavy atoms (18–108)	0.73±0.32
Heavy atoms (secondary structure)	1.30±0.25

Table 2

Kinetic parameters of wild type and C98S forms of MsrB2.

Protein	DTT-dependent reaction		Trx-dependent reaction	
	V_{max} (nmol/min/mg)	K_m (mM),	V_{max} (nmol/min/mg),	K_m (mM)
Wild-type	279 ± 10	0.03 ± 0.004	282 ± 35	0.66 ± 0.12
C98S	390 ± 55	0.05 ± 0.019	1760 ± 120	7.0 ± 0.4

Purified proteins were assayed in DTT- and Trx-dependent reactions in 50 mM sodium phosphate, pH 7.5, 50 mM NaCl. V_{max} and K_m values were determined by fitting the experimental data to the Michaelis-Menten equation.

Table 3

Activity of MsrB2 at different pH values.

Buffer	pH	Specific activity (nmol/min/mg protein)
Sodium phosphate	5.7	23
	6.5	55
	7.0	110
	7.5	228
Tris-HCl	7.6	119
	8.0	267
	8.6	446
	9.0	484
Carbonate-bicarbonate	9.2	462
	9.6	272
	10.0	74

The reaction mixture (100 μl) contained 100 mM sodium phosphate, 50 mM Tris-HCl, or 50 mM carbonate-bicarbonate with the indicated pH values, 200 μM dabsyl-Met-*R*-O, 20 mM DTT, and 1 μg MsrB2. The reaction was carried out at 37°C for 30 min and the product, dabsyl-Met, was analyzed by the established HPLC procedure.